THE JOURNAL OF PHYSICAL CHEMISTRY B

Article

pubs.acs.org/JPCB

Relating Structure, Entropy, and Energy of Solvation of Nanoscale Solutes: Application to Gold Nanoparticle Dispersions

Divya Nayar, Hari Om Sharanam Yadav, B. Shadrack Jabes, and Charusita Chakravarty*

Department of Chemistry, Indian Institute of Technology-Delhi, New Delhi 110016, India

ABSTRACT: Structural estimators for the entropy are combined with an analysis of the different contributions to the energy of solvation to understand the molecular basis of the thermodynamics of solvation of passivated nanoparticles. Molecular dynamics simulations of thiolated gold clusters in ethane are performed over a wide range of densities close to the critical isotherm. The entropic changes associated with solvent reorganization around the passivated nanoparticle are estimated from the nanoparticle−solvent pair correlation function, while the entropy of the ligand shell is estimated from the covariance in the positional fluctuations of the ligand atoms. The ligand-shell entropy (S_L) is shown to be fairly insensitive to variations in solvent density ranging from vacuum to twice the critical density (ρ_c). In contrast, the entropy change due to solvent reorganization (ΔS_{ns}^{ord}) shows a minimum around the critical point where the solvent excess shows a maximum. Combining the entropic estimates with the nanoparticle−solvent interaction energies, the free energy of solvation is shown to decrease with density once the critical point is crossed in a manner qualitatively consistent with available experimental data. The results suggest that such an approach to obtain structural insights into the thermodynamics of solvation of passivated nanoparticles could be useful in understanding the stability of nanoparticle dispersions of widely varying chemistries. This study also demonstrates that the theoretical analysis of solvation and self-assembly developed in the context of biomolecular hydration can be very usefully extended to understand the behavior of inorganic nanoparticle dispersions.

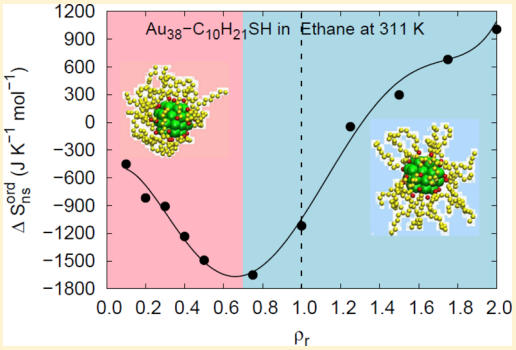

1. INTRODUCTION

Studies of the molecular basis of solvation typically consider either structureless solutes or small molecules[1−8] or complex biomolecular solutes, such as peptides.[9−15] Passivated inorganic nanoparticles represent a relatively new and interesting class of nanoscale solutes for which the thermodynamics of solvation is not well-understood. Stabilizing dispersions of passivated nanoparticles in suitable solvents is a necessary step in the synthesis of bulk nanostructured materials, such as polymer nanocomposites, thin films, and superlattices.[16−21] Nanocrystals of metals or semiconductors can be stabilized by passivating the surface with suitably chosen ligands. Despite the relative structural simplicity of passivated nanoparticles, the stability, rheology, and self-assembly of the nanoparticle dispersions are crucially dependent on the chemistry of the inorganic core, the ligands, and the solvent.[22,23] Like biomolecules, the entropy associated with the conformational degrees of freedom plays a significant role in the thermodynamics of solvation. In addition, unlike in the case of colloidal particles and like in the case of molecules, the structural length scale of the solvent is comparable to that of the nanoparticle, and therefore a microscopic modeling of solvent structure and dynamics is necessary.[24,25] To understand the thermodynamics of solvation of such macromolecules, it would be useful to be able to quantitatively relate entropic and energetic parameters for solvation with the reorganization of the ligand shell and the solvent surrounding the nanoparticle. In principle, structural estimators for the entropy and energy of solvation, developed in alternate contexts such as biomolecular hydration, can be adapted to understand solvation of ligand-passivated nanoparticles. In this study, we focus on applying some of these metrics to relate structural, entropic, and energetic changes associated with solvation of nanoparticles, using thiolated gold clusters in ethane as a prototypical example of such systems.

Ligand-protected gold nanoclusters display an interesting range of optoelectronic properties and are stable in a variety of nonpolar solvents.[16,17,19,26−29] Synthetic routes for the preparation of size-selected gold clusters in dispersive media are now well-established, and as a consequence, they form components in a variety of two- and three-dimensional self-assembled structures. Given the huge amount of experimental data available, an understanding of the principles and trends governing the relationship between the chemistry of the nanocrystal−ligand−solvent systems and the stability of nanoparticle dispersions and their subsequent self-assembly is an active area of research.[22,23,30,31] Atomistic simulation studies in the last ten years are starting to play an important role in developing correlations between chemistry, structure, and thermodynamics of such nanoscale systems. As in this study, the thiolated gold clusters are frequently chosen as prototypes for passivated nanoclusters since the interatomic interactions are sufficiently well-understood that acceptable parametric

Received: August 1, 2012
Revised: September 19, 2012
Published: September 21, 2012

potentials can be designed.[32−34,34−42] This study focuses specifically on the thermodynamics of solvation of gold−thiol nanoclusters in ethane. Experimental data are available on gold−octanethiol clusters in the size range of 1.5−6 nm in compressed ethane and propane in the supercritical region.[43,44] Previous simulation studies that examine density-dependent solvation behavior of alkanethiol gold clusters in supercritical ethane solvent focus largely on the solvent organization in the neighborhood of the gold−thiol nanocluster,[39,40,42] while this study focuses on relating this structural information to the thermodynamics of solvation.

Since this is an initial study to examine structure-based metrics related to energy and enthalpy of solvation, we have performed simulations of a small, 38-atom gold cluster with a diameter of approximately 1.2 nm. The nanocrystal geometry corresponds to the truncated octahedral fragment of the face-centered cubic lattice identified as the global minimum of the Murrell−Mortram potential for this cluster size.[45] Experimentally, large gold nanocrystals are known to be crystalline with some dependence of packing geometry and faceting on the method of preparation. In the case of small clusters, the strong sulfur−gold interactions can potentially cause significant structural reconstruction of the gold core.[39,40] Since the purpose of this study is to develop structural metrics for nanoparticle solvation, we have preferred to keep the gold core as a rigid, ordered structure with the global minimum energy geometry of the isolated metallic cluster, in keeping with several previous computational studies.[34−36,42] Passivation of this metallic core by butanethiol (C_4H_9SH) and decanethiol ($C_{10}H_{21}SH$) has been considered. The solvent was chosen to be ethane since thiolated gold clusters have significant solubility in supercritical ethane and varying the density of ethane provides a simple method for tuning the solvent quality. The paper is organized as follows. In Section 2, we review our approach to computing the thermodynamic parameters for solvation of a macromolecular solute, such as a passivated nanoparticle. Section 3 provides the computational details of the model and the molecular dynamics simulations. Section 4 describes our results, and Sections 5 summarizes the conclusions of this study.

2. THERMODYNAMICS OF SOLVATION OF PASSIVATED NANOPARTICLES

The work of Ben-Naim suggests that from the point of view of statistical thermodynamics the most appropriate standard state for a structureless solute is to fix its location in the solvent held at fixed density and temperature, thereby eliminating the solute translational contribution to the entropy.[1] The energetic and entropic changes on solvation, ΔU_{solv} and ΔS_{solv}, respectively, will then be associated with the reorganization of the solvent around the solute. In the specific case of thiolated gold nanoparticles, we assume that the metal atoms forming the rigid gold cluster are held fixed, thereby eliminating the translational and rotational motion of the solute. The mobile alkyl chains of the ligands are, however, free to reorganize under the influence of the solvent, thereby resulting in intra-solute reorganizational contributions to solvent energy and entropy. For the pair-additive potentials used in this study, computing the contributions due to interactions between the gold core (n), the ligands (L), and the solvent (s) is straightforward. The configurational energy of interaction between the passivated nanoparticle and the solvent will be given by the sum of gold−solvent, ligand−solvent, gold−ligand, and ligand−ligand interactions, denoted by U_{n-s}, U_{L-s}, U_{n-L}, and U_{L-L}, respectively. In the case of the thiolated gold nanoparticles, the intra-solute gold−ligand (U_{n-L}) and ligand−ligand (U_{L-L}) interactions are relatively insensitive to changes in solvent density, and we can approximate the internal energy change on solvation as

$$\Delta U_{solv} = \Delta U_{ns} = U_{n-s} + U_{L-s} \tag{1}$$

We note that in other systems, with more complex solvent−ligand chemistries or low grafting densities, it may be necessary to take these terms into account.

The entropy change on solvation can, in principle, be evaluated using free energy estimation approaches.[41] Structural estimators for the entropy, dicussed here, provide a molecular level understanding of these entropy changes. The free energy changes to solvation will be dominated by ligand−solvent interactions since the inorganic core is expected to be relatively rigid and is not expected to undergo significant structural reorganization due to solvent effects. We denote the entropy associated with the ligand shell by S_L, and in Section 2.1, we define a structural estimator for this quantity that has been widely used for biomolecular systems.[9−11,46] The entropy associated with solvent reorganization in the presence of the solute is denoted by S_{ns}^{ord} and is evaluated using a pair correlation based approach discussed in Section 2.2.

2.1. Entropy of the Ligand Shell. We first consider the entropy of the ligand shell or corona surrounding the metallic core. This corona of flexible, long-chain molecules interacts with the solvent and may be expected to undergo significant reorganization on solvation. A simple and physically appealing structural metric to measure the entropy associated with the ligand shell organization is based on the covariance in particle displacements of ligand atoms. This method was developed by Schlitter and others to compute the configurational entropy of biomolecules in aqueous media.[9−11,46] An upper bound to this ligand configurational entropy, S_L, can be estimated by calculating the covariances of the Cartesian coordinates of atoms of the ligand molecules using the expression

$$S_L = \frac{1}{2}k \ln \det\left[1 + \frac{kTe^2}{\hbar}\mathbf{M}^{1/2}\sigma\mathrm{M}^{1/2}\right] \tag{2}$$

where k is Boltzmann constant e is Euler number which is equal to exp(1); $\mathbf{M}$ is the $3N$-dimensional diagonal matrix having masses of N atoms of decanethiol chains; T is the temperature of the simulation; and σ is the covariance in positions of the atoms of ligand chains. The covariance in atomic positions can be defined as

$$\langle\sigma_{ij}\rangle = \langle(x_i - \langle x_i\rangle)(x_j - \langle x_j\rangle)\rangle \tag{3}$$

where x_i and x_j are the Cartesian coordinates of the ith and jth atoms. Note that the Schlitter entropy (S_L), as defined above, is an upper bound to the entropy associated with the ligand shell.

The Schlitter entropy metric estimates, within the quasiharmonic approximation, the entropy associated with the ligand shell, S_L. The entropy change due to reorganization of the ligand in the presence of the solvent at density ρ will be given by $\Delta S_L = S_L(\rho) - S_L(\rho = 0)$.

2.2. Entropy Due to Solvent Reorganization around a Solute. In this section, we derive the expression for the pair correlation contribution to the solvation entropy of the solute at infinite dilution, following the approach of Lazaridis.[6,7] We make a crucial approximation when deriving this solvent

ordering entropy of neglecting the internal structure of the passivated nanoparticle and therefore implicitly partitioning the entropy contribution into a ligand shell contribution, discussed above, and an independent solvent reorganization term. An additional point to be noted is that even though the solvent in this case is ethane we consider the pair correlation function between the solvent methyl groups and the center of the nanoparticle core. This should be useful in comparing solvation effects in different alkane solvents in future work since monomer-dependent pair correlation terms are useful in understanding the structure and dynamics of chain fluids, such as alkanes.[47]

Consider a system consisting of a mixture of N_n solute (passivated nanoparticle) and N_s solvent atoms (methyl groups) in a volume V. The ensemble-invariant form of the entropy due to ideal and pair entropy contribution is given by[48,49]

$$\begin{aligned} S = {} & N_n[(5/2)k - k\ln(\rho_n\Lambda_n^3)] + N_s[(5/2)k - k\ln(\rho_s\Lambda_s^3)] \\ & - kN_n\rho_s\int(g_{ns}\ln g_{ns} - g_{ns} + 1)\mathrm{d}\mathbf{r} - 1/2kN_n \\ & \rho_n\int(g_{nn}\ln g_{nn} - g_{nn} + 1)\mathrm{d}\mathbf{r} - 1/2kN_s \\ & \rho_s\int(g_{ss}\ln g_{ss} - g_{ss} + 1)\mathrm{d}\mathbf{r} \end{aligned} \tag{4}$$

where ρ_n and ρ_s are the solute and solvent densities, respectively; Λ_n and Λ_s are the thermal de Broglie wavelengths of the two species; and g_{ss}, g_{ns}, and g_{ss} are the solvent−solvent, solute−solvent, and solvent−solvent pair correlation functions, respectively. The above expression neglects the three-body and higher-order terms in the multiparticle correlation expansion of the entropy of the fluid mixture. In simple liquids, dominated by pair interactions, the contribution of these neglected terms is approximately 10−20% of the pair entropy. We expect that given the nature of the intermolecular interactions in the gold−thiol−alkane system similar numbers will apply as in the case of simple liquids. These terms may be more significant in other systems where three-body correlations controlling solvent−solvent correlations in the presence of a solute are significant.

The entropy of solvation at infinite dilution will be obtained by taking the partial derivative, $(\partial S/\partial N_n)$, in the infinite dilution limit when the $\rho_n \to 0$ and $N_n \to 1$. We focus on taking the derivatives of the first three terms of eq 4. The fourth term will not be relevant at infinite dilution. The derivative with respect to N_n of the last term will correspond to the pair correlation contribution to the solvent reorganization entropy in the presence of a solute and will not be considered here. By defining the partial molar volume of the solute at infinite dilution as

$$\overline{v}_n^{\infty} = (\partial V/\partial N_n)_{T,P,\rho_n\to 0} \tag{5}$$

we then obtain

$$\begin{aligned} (\partial S/\partial N_n)_{T,P} = {} & [(5/2)k - k\ln(\rho_n\Lambda_n^3)] + k\rho_n\overline{v}_n^{\infty} \\ & - k + k\rho_s\overline{v}_n^{\infty} - k\rho_s\int(g_{ns}\ln g_{ns} - g_{ns} + 1)\mathrm{d}\mathbf{r} \\ & + k\rho_n\rho_s\overline{v}_n^{\infty}\int(g_{ns}\ln g_{ns} - g_{ns} + 1)\mathrm{d}\mathbf{r} \end{aligned} \tag{6}$$

Since $\rho_n \to 0$ in the inifinite dilution limit, within the pair correlation approximation, the entropy of solvation of the nanoparticle solute at infinite dilution is given by

$$\begin{aligned} \overline{S}_n^{\infty} = {} & [(5/2)k - k\ln(\rho_n\Lambda_n^3)] - k(1 - \rho_s\overline{v}_n^{\infty}) \\ & - k\rho_s\int(g_{ns}\ln g_{ns} - g_{ns} + 1)\mathrm{d}\mathbf{r} \\ = {} & [(3/2)k - k\ln(\rho_n\Lambda_n^3)] + k\rho_s\overline{v}_n^{\infty} \\ & - k\rho_s\int(g_{ns}\ln g_{ns} - g_{ns} + 1)\mathrm{d}\mathbf{r} \end{aligned} \tag{7}$$

The partial molar volume of an infinitely dilute solute in a binary mixture is given by[3]

$$\overline{v}_n^{\infty} = kT\kappa_T - \int(g_{ns} - 1)\mathrm{d}\mathbf{r} \tag{8}$$

Using this definition of $\overline{v}_n^{\infty}$ in the equation of entropy, one can rewrite in units of the Boltzmann constant k as

$$\begin{aligned} \overline{S}_n^{\infty}/k = {} & [(3/2) - \ln(\rho_n\Lambda_n^3)] + \rho_s kT\kappa_T \\ & - \rho_s\int(g_{ns}\ln g_{ns})\mathrm{d}\mathbf{r} \end{aligned} \tag{9}$$

The first term in the above expression is the entropy associated with translational motion of the center of mass of the solute which will be irrelevant in the Ben-Naim formulation of the local standard quantities for solvation. The second term clearly depends on the properties of the bulk solvent. The third term is the contribution to solvation entropy due to local ordering of the solvent in the neighborhood of the solute and will be zero in the vacuum. The entropy change associated with solvent reorganization when a solute is moved from the vacuum to a fixed location on the solvent will therefore be given by

$$\Delta S_{ns}^{ord}/k = -\rho_s\int(g_{ns}\ln g_{ns})\mathrm{d}\mathbf{r} \tag{10}$$

Assuming a spherically symmetric solute structure, this may be written as

$$\Delta S_{ns}^{ord}/k = -4\pi\rho_s\int(g_{ns}\ln g_{ns})r^2\mathrm{d}\mathbf{r} \tag{11}$$

Note that the solute−solvent pair correlation function used here for the solvated gold nanoparticle corresponds to the correlation between the center of mass of the gold core and the methyl groups of fluid ethane used as solvent, thereby avoiding orientation-dependent pair correlation functions for a diatomic solvent such as ethane.

In this context, it is useful to recollect that the solvent excess, n_s^E, is a quantitative measure of the affinity of the solute for the solvent and is related to $g_{ns}(r)$ in terms of the Kirkwood−Buff integral[50]

$$n_s^E = 4\pi\rho_s\int_0^{\infty}(g_{ns}(r) - 1)r^2\mathrm{d}r \tag{12}$$

It can be defined as the excess number of solvent molecules (methyl groups) around an infinitely dilute solute molecule.[2,3] Equation 12 shows that it will have a strong dependence on solvent compressibility and therefore will increase dramatically in the neighborhood of the solvent critical point.[39,40,51] It may be noted that in an earlier study of thiolated gold nanoparticles the solvent excess was computed per gold atom of the nanoparticle.[39,40]

The discussion in this section can be summarized by noting that the solubility will depend on the free energy of solvation of

a given solute. The analysis of Yu and Karplus suggests that the free energy of solvation should contain only the local contributions to the entropy and the internal energy and therefore can be written as[5,8]

$$\Delta A_{solv} = \Delta U_{solv} - T\Delta S_{solv} \quad (13)$$

The internal energy change on solvation for our passivated nanoparticle in solution is denoted by ΔU_{solv} as defined in eq 1. The entropy change on solvation will be given by

$$\Delta S_{ns} = \Delta S_{ns}^{ord} + \Delta S_{L} \quad (14)$$

where the first term is due to a change in the local structure of the solvent due to the solute and the second term is due to the change in the structure of the solute due to the solvent. The free energy change associated with solvation of the nanoparticle using the structural estimators defined in this section will be given by

$$\Delta A_{ns} = \Delta U_{ns} - T\Delta S_{ns}^{ord} - T\Delta S_{L} \quad (15)$$

3. COMPUTATIONAL DETAILS

3.1. Potential Energy Surface. This section describes the functional form and parametrization of the potential energy surface used for the thiolated Au_{38} gold cluster in ethane in this study. The details are essentially identical to those used in the earlier study by Patel and Egorov.[42] We also note that the same functional form but with a different choice of parameter values was used in a study by Tay and Bresme.[34]

The united atom version of TraPPE potential is used for the ethane solvent where the methyl groups are represented by Lennard-Jones spheres connected by a rigid bond.[52] The potential parameters and the bond lengths are given in Tables 1 and 2. The critical parameters for the solvent obtained with this model are ρ_c = 0.206 g cm^{-3}, T_c = 304 K, and P_c = 5.1 MPa which may be compared with experimental values of 0.203 g cm^{-3}, 305 K, and 5.9 MPa, respectively.[52]

Table 1. Potential Parameters for the Passivating Alkyl Chains[a]

interaction type	interacting group	potential parameters[b]
rigid bond	CH_x–CH_x	l_0 = 1.54
	CH_2–SH	l_0 = 1.82
bond bending	CH_2–CH_2–CH_x;	k_0 = 519.73
	CH_2–CH_2–SH	θ_0 = 114.40
bond torsion	CH_2–CH_2–CH_2–SH;	A_1 = 5.9046
	CH_2–CH_2–CH_2–CH_x	A_2 = −1.1340
		A_3 = 13.1608

[a]Equilibrium bond length is denoted by l_0. Bond angles are modeled using harmonic potential: $U(\theta) = ((1/2)k_\theta)(\theta - \theta_0)^2$, where k_θ is the force constant and θ_0 is the equilibrium bond angle. OPLS triple cosine potential is used for torsional interactions given by: $U(\phi) = (1/2)A_1(1 + \cos(\phi)) + (1/2)A_2(1 - \cos(2\phi)) + (1/2)A_3(1 + \cos(3\phi))$ where A_1, A_2, and A_3 are constants. The parameters are taken from references 34 and 42. [b]The units of distance are in Angstrom, angles in degrees, and energy in kJ/mol.

Table 2. Lennard-Jones Parameters for Nonbonded Interactions for the Thiolated Gold Particles in Alkane Solvent[a]

atom pairs	ε (kJ mol^{-1})	σ (Å)
CH_2	0.3825	3.950
CH_3	0.8148	3.750
SH	1.6629	4.450
Au	3.2288	2.737

[a]The CH_2 and CH_3 parameters are taken from the TraPPE-UA potential,[52] and the SH and Au parameters are taken from references 33, 34, and 42.

The 38-atom gold core is assumed to be a truncated octahedral fragment of a face-centered cubic lattice. We have used the global minimum structure predicted by Wilson and Johnston using the empirical Murrell–Mottram potential.[45] The nearest neighbor distance with this potential is 0.284 nm, and the overall cluster diameter may therefore be estimated to be 1.16 nm. This may be compared with the smallest cluster size of 1.5 nm for which experimental solubility data are available.[43,44] Since the gold cluster is held rigid, no Au–Au interaction potential is required for our simulations.

The alkylthiols are modeled using a united atom approach, as in the case of ethane, with SH, CH_2, and CH_3 represented by pseudoatoms. Nonbonded interactions between these pseudoatoms are modeled by Lennard-Jones parameters, either those given in Table 2 or, in the case of dissimilar atom pairs, by suitable application of the Lorentz–Berthelot combining rules.[53] Adjacent pseudo-atomic ligand segments were assumed to be held by rigid bonds with bond lengths given in Table 1. A harmonic potential was used for the bond angle vibrations, and four-body torsions were modeled using the OPLS triple cosine potentials.[54−56] The gold–sulfur linkage between the metal core and the alkylthiol interactions is modeled by an effective nonbonded, short-range m–n potential represented as[34,57,58]

$$U(r_{ij}) = \frac{E_0}{n-m}\left[m\left(\frac{r_0}{r_{ij}}\right)^n - n\left(\frac{r_0}{r_{ij}}\right)^m\right] \quad (16)$$

where E_0 = 38.6 kJ/mol; n = 8; m = 4; r_0 = 2.9 Å; and the potential is truncated and shifted at 6.2 Å cutoff. The simulations in this study were performed using either *n*-butanethiol or *n*-decanethiol passivating ligands.

3.2. Passivation of Gold Core in a Vacuum. As an initial step in the simulation, it is necessary to carry out the passivation of the bare gold cluster by the appropriate ligands in vacuum. We use a protocol similar to that followed by Luedtke and Landman.[32,33] The coordinates of the Au_{38} cluster were taken from references 45 and 59. The cluster was placed at the center of a 50 Å × 50 Å × 50 Å cubic cell and packed randomly with 100 decanethiol chains around the gold nanoparticle using the PACKMOL package.[60] The molecular dynamics simulations of this single cluster in a vacuum were carried out using the DL_POLY package.[61] The velocity Verlet algorithm with a time step of 1 fs was used to integrate the equations of motion. Bond constraints were applied using the RATTLE algorithm. The Au_{38} core was kept *frozen* during the simulations which corresponds to keeping the core atoms at a fixed position in the simulation cell by setting all velocities and forces of atoms to zero during the simulation.[61] This system of the Au_{38} cluster packed with decanethiol chains was allowed to equilibrate for a period of 2.5 ns at 200 K. To ensure equilibriation, forces were capped at $1000k_BT$/Å, and rescaling of velocities was performed every 50 time steps. The system thus obtained was heated gradually using NVE (microcanonical) run lengths of 1 ns each, with temperature changing from 200 to 500 K in steps of 50 K. The temperature change corresponded to resampling the velocities from the approximate thermal distribution at the start

dx.doi.org/10.1021/jp307615f | J. Phys. Chem. B 2012, 116, 13124−13132

of each 1 ns run. The system was then similarly cooled back to 300 K using 1 ns runs with temperature changing in steps of 50 K each. The slow heating followed by cooling allows for both diffusion of ligands on the cluster surface and desorption of any excess ligands and allows the system to find the basin of the global minimum. At the end of this passivation protocol, the number of decanethiol chains attached to the gold core was 24, which is consistent with the number of binding sites available for optimal attachment of thiols on the surface of the cluster. The excess chains were removed from the simulation cell, and a small, 1 ns simulation was performed to ensure that no further desorption of the adsorbed decanethiol chains took place. The butanethiol cluster was obtained from the equilibrated decanethiol cluster by removing the CH_2 groups one by one and equilibrating the system on removal of each CH_2 group.

To obtain the properties of the passivated nanoparticle at zero solvent density, an equilibration run of 2.5 ns of the passivated single nanoparticle was performed in vacuum at 311 K followed by a production run of the same length. Simulation of a single nanoparticle at 350 K in vacuum was done following the heating protocol as described above, followed by similar equilibration and production runs.

3.3. Solvation of Passivated Nanoparticles. Once the gold cluster was passivated, the initial configuration for each of the densities was prepared by placing the passivated gold cluster at the center of the box and adding the appropriate number of ethane molecules randomly without any overlaps in a cubic box (100 Å × 100 Å × 100 Å) using the PACKMOL software. Subsequent equilibriation and production runs were carried out using the DL_POLY molecular dynamics simulation code.

The equations of motion were integrated using the velocity Verlet integrator algorithm with bond constraints implemented with the RATTLE algorithm. Simulations were carried out for temperatures 311 and 350 K with different densities ranging from $0.1\rho_c$ to $2.0\rho_c$ (where ρ_c = critical density of bulk solvent, 0.206 g cm^{-3}). The passivated gold core solvated at different solvent densities was first equilibrated for about 2.5 ns at 311 K, capping all the forces. Another equilibration run for 2.5 ns, without capping the forces, was performed. Simulation study of solvation at 350 K for each of the densities was done taking the equilibrated configuration of 311 K. The equilibrated system obtained at 311 K was heated gradually (as described previously), using runs of 1 ns each with temperature changing from 311 to 360 K in steps of 10 K each. It was cooled gradually using 1.0 ns runs with temperature changing from 360 to 350 K in steps of 2 K each. Once the system reached the desired temperature, equilibration was done with rescaling of velocities every 50 steps for 2.5 ns. Microcanonical ensemble production runs of 2.5 ns were then carried out with a time step of 1 fs. No obvious inhomogeneities were observed in the system during simulations. As a check for equilibration of the system in the NVE ensemble, we have calculated Tuckerman's energy conservation parameter[62] for all the densities and temperatures, and it was found to be of the order of 10^{-4} to 10^{-5}.

In the vacuum simulations, it was necessary to hold the gold core frozen, to avoid problems with equilibriation due to the slow rotational motion of the gold core. For the solvated nanoparticle, even at low densities, the molecular dynamics simulations with the rigid, as well as frozen, core gave results that matched with those of Patel et al. for structural properties.[42]

3.4. Estimation of Entropic Contributions to Solvation Due to Ligand and Solvent. As described in the previous section, the ligand configurational entropy of the ligand chains is calculated by using the covariance in atomic positions of the ligand chain groups (SH, CH_2, and CH_3 groups). The definition of this entropy involves computing the determinant of the following matrix

$$\left[1 + \frac{kTe^2}{\hbar}\mathbf{M}^{1/2}\sigma\mathbf{M}^{1/2}\right] \tag{17}$$

which is a symmetric and positive-definite matrix. We have used Cholesky's decomposition method to compute its determinant.[11] In this method, the matrix is decomposed into a lower triangular matrix L whose transpose acts as the upper triangle matrix, i.e., $A = LL^T$. The determinant of the matrix A, therefore, is a product of squares of diagonal elements of matrix L.

The trajectories obtained from production runs were used to compute the covariance matrix, σ. In Figure 1, we show the convergence of S_L as a function of length of trajectory for the butanethiol−gold cluster at 311 K and the decanethiol−gold cluster at 311 and 350 K. For the system with butanethiol chains, production runs of 2.5 ns were sufficient to obtain converged entropy value. In the case of the longer-chain decanethiol−gold cluster, the convergence with trajectory length is rapid until approximately 4 ns and is then followed by a very slow convergence. However, the difference between S_L values of the decanethiol system at 311 and 350 K stays almost constant, suggesting that run lengths of 10 ns are sufficient for estimating relative entropy differences. The results in Table 3 therefore have been obtained by averaging over a 10 ns production run trajectory for the system having decanethiol chains at 311 and 350 K. For the estimation of entropic contributions to solvation due to solvent reorganization around the nanoparticle, we have computed ΔS_{ns}^{ord}, making use of the radial distribution function $(g_{ns}(r))$ as defined in Section 2.2.

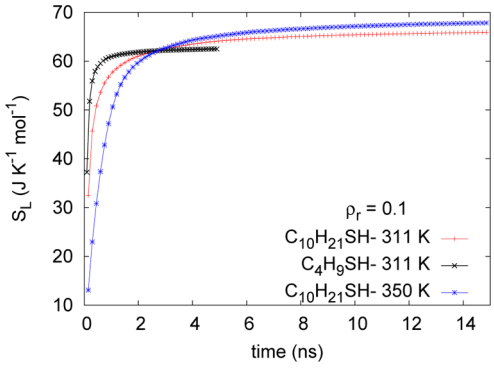

Figure 1. Cumulative ligand configurational entropy per (CH_x/SH) group, S_L, of the alkyl chain atoms (SH, CH_2 and CH_3 groups) in the solvated and passivated Au_{38} system having reduced solvent density of $0.1\rho_c$ as a function of time at 311 and 350 K.

4. RESULTS AND DISCUSSION

4.1. Ligand-Shell Structure and Entropy. The structure of the ligand shell can be characterized by the radial density profile of the ligand chain monomers with respect to the center of mass of the gold core. Figure 2 shows the $\rho_L(r)$ values at nine densities spanning the density range from 0 to $2\rho_c$ at 311

dx.doi.org/10.1021/jp307615f | J. Phys. Chem. B 2012, 116, 13124−13132

Table 3. Radius of Gyration between the Gold Center of Mass and CH_2 Groups of the Passivating Alkyl Chains and the Ligand Configurational Entropy per (CH_x/SH) Group of the Alkyl Chains at 311 and 350 K[a]

		R_g (Å)			S_L (J K^{-1} mol^{-1})		
		311 K		350 K	311 K		350 K
ρ (g cm^{-3})	ρ/ρ_c	$C_{10}H_{21}SH$	C_4H_9SH	$C_{10}H_{21}SH$	$C_{10}H_{21}SH$	C_4H_9SH	$C_{10}H_{21}SH$
0.0000	0.00	10.6	8.6	10.7	66.3	63.3	68.3
0.0206	0.10	10.7	8.6	10.8	65.9	63.0	68.2
0.0412	0.20	10.9	8.6	10.9	65.5	63.2	68.2
0.0618	0.30	10.9	8.6	10.9	65.6	63.2	67.8
0.0824	0.40	10.9	8.6	11.0	65.4	62.9	68.1
0.1030	0.50	11.1	8.6	11.0	65.1	63.1	68.1
0.1545	0.75	11.1	8.6	11.1	65.0	62.9	68.0
0.2060	1.00	11.2	8.7	11.2	65.2	62.8	67.8
0.2575	1.25	11.2	8.7	11.2	65.3	62.8	68.2
0.3090	1.50	11.2	8.7	11.2	65.4	62.6	68.0
0.3605	1.75	11.2	8.6	11.2	64.8	62.4	67.8
0.4120	2.00	11.3	8.7	11.3	65.0	62.3	67.7

[a]Also shown are the values for the passivated nanoparticle in vacuum at 311 and 350 K.

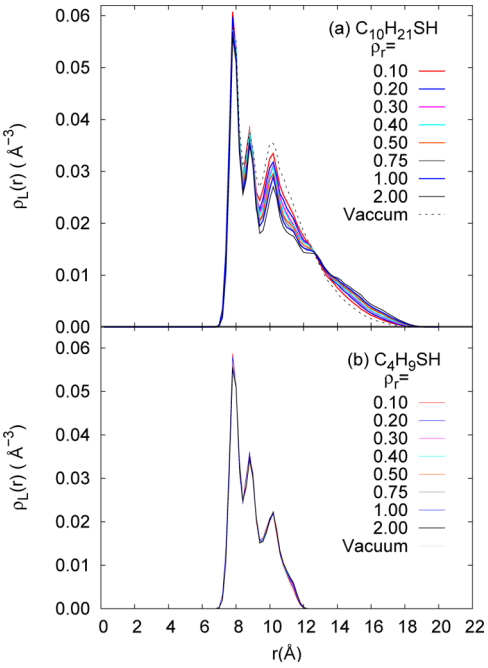

Figure 2. Radial density profiles ($\rho_L(r)$) of ligand chain monomers (for CH_2 and CH_3 groups only) for the system of the Au_{38} nanoparticle passivated with (a) $C_{10}H_{21}SH$ and (b) C_4H_9SH alkyl chains at 311 K at different reduced solvent densities ($\rho_r = \rho/\rho_c$).

K, along the critical isotherm. It is evident that in the case of butanethiol the ligand corona is compact and insensitive to variations in solvent density. In the case of the longer chain decanethiol ligands, the solvent penetration into the ligand shell is greater, and it is evident that the outer regions of the ligand shell are sensitive to the solvent density. Table 3 shows the radius of gyration and the Schlitter estimate of the ligand shell entropy due to positional fluctuations. The radius of gyration has been computed here as the average distance of the methylene (CH_2) groups of all the ligand chains from the center-of-mass of the gold nanoparticle, excluding both sulfur and terminal methyl groups. This provides a reasonable single measure of the effective extent of the ligand shell.

The Schlitter entropy for the thiolated gold clusters seems insensitive to density, within statistical error, and shows only a weak dependence on temperature. This may be due to the fact that the structure of the ligand shell as well as the solvent is dominated by packing of the pseudoatomic CH_2/CH_3 groups and is therefore insensitive to variations in solvent density. The ability of the Schlitter entropy metric to discriminate between folded and unfolded structures of proteins and peptides, however, suggests that this metric may be more useful in judging the effects of varying grafting density, ligand branching, and chemistry of the ligand−solvent systems.

4.2. Solvent Reorganization around Passivated Nanoparticle. Figure 3 shows the pair correlation function, $g_{ns}(r)$,

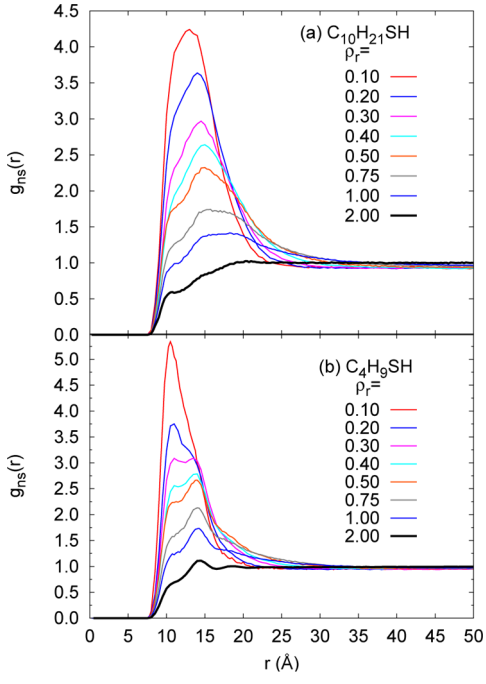

Figure 3. Pair correlation function, $g_{ns}(r)$, between methyl groups of ethane solvent and the center of mass of the gold nanoparticle for the system of a Au_{38} core passivated with (a) $C_{10}H_{21}SH$ chains and (b) C_4H_9SH alkyl chains at 311 K at various reduced solvent densities.

dx.doi.org/10.1021/jp307615f | J. Phys. Chem. B 2012, 116, 13124−13132

corresponding to the probability of finding a solvent methyl group at a distance r from the center of mass of the gold core. For $\rho \leq \rho_c$, a well-defined solvation layer with $g_{ns} > 1$ in the nighbourhood of the solute is identifiable. Comparison with Figure 2 shows that the solvent molecules prefer to localize within the ligand shell in the neighborhood of the gold core, presumably because of favorable attractive interaction with the ligand methyl and methylene groups. The structuring of this solvent layer is more apparent for the short butanethiol chains rather than for the longer decanethiol chains. For $\rho > \rho_c$, it is apparent that the solvent density is lower in the first layer; i.e., the bulk solvent density is sufficiently high that the solvent molecules do not localize in the neighborhood of the ligand shell.

We first consider the solvation of the decanethiol-coated Au_{38} nanoparticle along the critical isotherm at 311 K. In Figure 4(a), we compute the solvent excess in the neighborhood of the

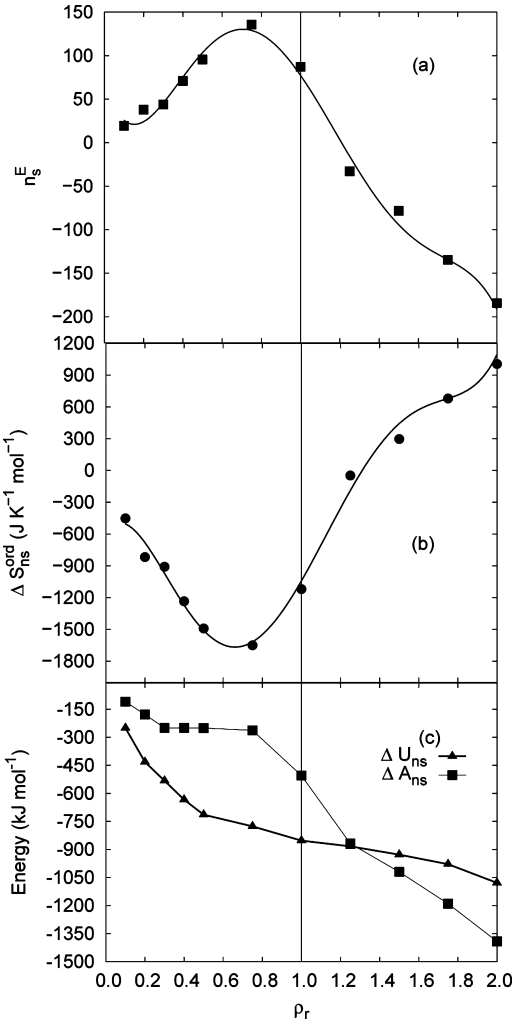

Figure 4. Relationship between structure, entropy, and energy for the system of Au_{38} passivated with $C_{10}H_{21}SH$ chains at 311 K. Part (a) shows the solvent excess number (n_s^E), (b) the solute−solvent ordering pair entropy (ΔS_{ns}^{ord}), and (c) shows the solvation free energy (ΔA_{ns}) and the average solute−solvent interaction energy (ΔU_{ns}) as a function of reduced solvent densities. The vertical line indicates critical density of the solvent.

passivated nanoparticle which reflects these changes in $g_{ns}(r)$. It is evident that for densities lower than the critical density the solvent excess is positive, while at high densities it is negative, with a crossover taking place at approximately ρ_c. Our results show that the passivated nanoparticle has an attractive solute−solvent interaction, as would be intuitively expected from experimental results, and this leads to an enhancement of local solvent concentration around the solute as expected on the basis of theoretical studies of solvation in near-critical solvents.[2,51]

We note that this quantity was earlier computed by Moti Lal et al. who found that passivation reduced the solute−solvent affinity.[39,40] The crucial difference between their study and ours as well those in refs 34 and 42 is that in our study the gold core is held rigid and is not allowed to distort significantly due to strong sulfur−gold interactions. It would appear that distortion of the gold core exposes the solvent to relatively unfavorable metal−gold interactions, and this may be responsible for lowering the solvent−nanoparticle affinity. The electronic structure calculations on the thiol−gold interactions are not as yet sufficiently conclusive as to the extent of distortion of the gold core due to Au−S interactions as a function of nanocrystal size and extent of thiol coverage.[63] Experimental results indicate that passivated gold nanoparticles above 2 nm size have well-ordered crystalline cores. The entropy change due to local ordering of the solvent in the neighborhood of the passivated nanoparticle, denoted by ΔS_{ns}^{ord}, is shown in Figure 4(b) as a function of density. In a qualitative sense, it is anticorrelated with the behavior of the solvent excess as a function of density, with a minimum in the near-critical region around $\rho_c \approx 0.8$ where n_s^E shows a maximum. Clearly, the progressive concentration of the solvent within the passivating layer increases with increasing density for $\rho < \rho_c$ and results in this negative contribution to the solvation entropy. At higher densities, the solvent ordering contribution to the entropy decreases with increasing density, as it becomes energetically and entropically more favorable for the solvent molecules to maximize favorable solvent−solvent attractions in a more dense bulk solvent.

4.3. Energy and Free Energy Changes on Solvation. In Figure 4(c), we show, as a function of density, both the energy change due to solvation as well as the Helmholtz free energy change on solvation. In computing ΔA_{ns}, we have neglected the ligand contribution, which for the thiolated gold clusters studied here is essentially insensitive to density. The $\Delta U_{ns}(\rho)$ function shows an initial pronounced decrease with increasing density presumably due to favorable solvent−ligand inetractions. For $\rho > 0.6\rho_c$ corresponding to the peak in the solvent excess, we find that ΔU_{ns} is almost constant with density. The minimum in ΔS_{ns}^{ord} and the maximum in n_{exc} therefore reflect clustering due to critical fluctuations. The Helmholtz free energy ΔA_{ns} is almost constant until the minimum in ΔS_{ns}^{ord} is reached and then decreases smoothly with temperature. This is qualitatively consistent with experimental results, demonstrating the increase in solubility of thiolated gold nanoparticles in compressed ethane as a function of increasing density.[43,44]

4.4. Effect of Chain Length and Temperature on Thermodynamics of Solvation. To gauge the usefulness of the structural metrics defined above for understanding the solvation of passivated nanoparticles, we show in Figure 5 and Table 3 some initial results regarding the effect of ligand chain lengths and temperature. A comparison of the gold cluster passivated with butanethiol and decanethiol indicates that even though the radius of gyration of the butanethiol−gold cluster is significantly smaller than that of the decanethiol cluster the

dx.doi.org/10.1021/jp307615f | J. Phys. Chem. B 2012, 116, 13124−13132

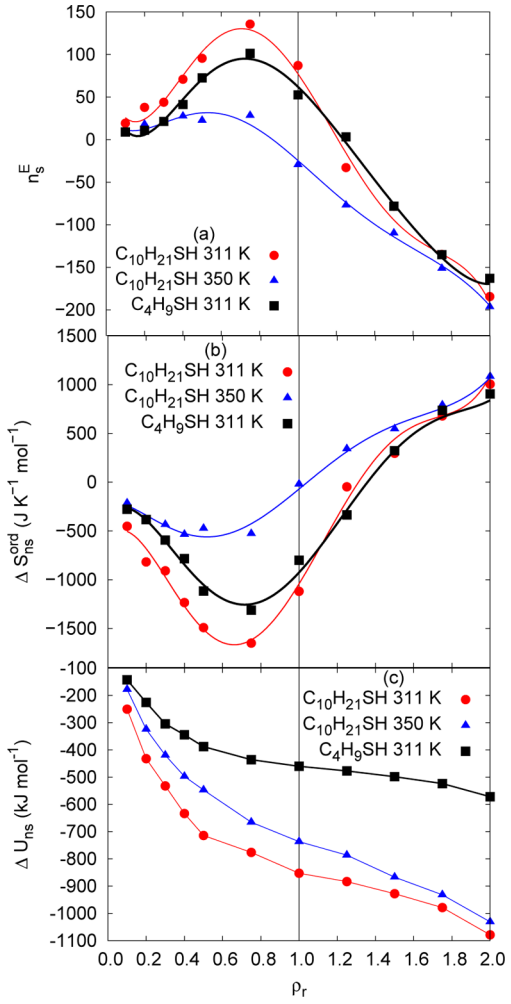

Figure 5. Comparison of the effect of alkyl chain length and temperature on (a) solvent excess number (n_s^E), (b) the solute–solvent ordering pair entropy (ΔS_{ns}^{ord}), and (c) average solute–solvent interaction energy (ΔU_{ns}) as a function of reduced solvent densities at 311 and 350 K. Vertical line indicates critical density of the solvent.

ligand shell entropy per methylene (or thiol) group is only 10% less for the shorter alkylthiol chain. The solvent excess function and the solvent ordering entropy of the butanethiol cluster are marginally less sensitive than the decanethiol cluster to variations in solvent density along the critical isotherms. In contrast, the nanoparticle–solvent interaction energy for the butanethiol cluster is much higher than the corresponding decanethiol system and shows less variation with density. We also compare the behavior of the decanethiol–gold cluster at 311 and 350 K. The deviation from the critical isotherm implies that the maximum in the solvent excess function and the minimum in the solvent ordering entropy are significantly less pronounced, while the change in the nanoparticle–solvent interaction energy is, however, qualitatively the same.

5. CONCLUSIONS

Molecular dynamics simulations of thiolated Au_{38} gold clusters in ethane are performed close to the critical isotherm over a wide range of densities, ranging from zero to twice the critical temperature ($2\rho_c$). The $(C_{10}H_{21}SH)_{24}Au_{38}$ cluster is studied at 311 and 350 K, and the $(C_4H_9SH)_{24}Au_{38}$ cluster is studied at 311 K.

The entropy of the ligand shell is estimated from the covariance in the positional fluctuations of the ligand atoms. The ligand-shell entropy (S_L) per CH_x/SH group is shown to be fairly insensitive to variations in solvent density ranging from vacuum to twice the critical density (ρ_c), with a variation of less than 2% as the solvent density increases from 0 to $2\rho_c$. The variations in the ligand shell entropy per methylene (or thiol) group are consistently less by about 5% for the butanethiol system, compared to the decanethiol system. The increase in ligand shell entropy, as estimated by the covariance approach, is found to be of the order of 5% for an approximately 40 K rise in temperature. These entropy changes are consistent with the changes in radius of gyration and radial density profiles of ligand monomers around the gold core.

The entropic changes associated with solvent reorganization around the passivated nanoparticle are estimated from the nanoparticle–solvent pair correlation function and show a very significant, nonmonotonic change as density varies from 0 to $2\rho_c$, especially along the near-critical isotherm at 311 K. The entropy due to solvent reorganization (ΔS_{ns}^{ord}) shows a minimum around the critical point where the solvent excess shows a maximum. The longer-chain length of the decanethiol–gold cluster, compared to the butanethiol cluster, results in a more pronounced variation in solvent reorganization entropy with density. The role of critical fluctuations in controlling the nonmonotonic behavior of the solvent ordering entropy can be seen in that on raising the temperature from 311 to 350 K, the maximum in solvent excess and minimum in solvent ordering entropy become less pronounced.

The configurational or internal energy change associated with solvent–nanoparticle interactions shows a steep initial decrease as density increases from vacuum to approximately $0.6\rho_c$ and then decreases relatively slowly with density. Combining the entropic estimates with the nanoparticle–solvent interaction energies, the free energy of solvation is shown to decrease with density once the critical point is crossed in a manner qualitatively consistent with available experimental data.

Our results suggest that the structural estimators for the entropy of solvation of passivated nanoparticles can provide significant structural insights into the thermodynamics of solvation of such macromolecular solutes and could be useful in understanding the stability of nanoparticle dispersions of widely varying chemistries. A more general point that emerges from this study is that the theoretical analysis of solvation and self-assembly developed in the context of biomolecular hydration can be very usefully extended to understand nanoparticle self-assembly.

AUTHOR INFORMATION

Corresponding Author

*E-mail: charus@chemistry.iitd.ac.in; charusita@gmail.com.

Notes

The authors declare no competing financial interest.

ACKNOWLEDGMENTS

The authors would like to thank Computer Services Centre, Indian Institute of Technology-Delhi, for their support. D.N. and H.O.S.Y. would like to thank the Council of Scientific and Industrial Research for the award of Senior Research Fellowship and Junior Research Fellowship, respectively. B.S.J. would

like to thank Indian Institute of Technology-Delhi for the award of a Senior Research Fellowship.

REFERENCES

(1) Ben-Naim, A. *J. Phys. Chem.* **1978**, *82*, 792−803.
(2) Petsche, I. B.; Debenedetti, P. G. *J. Chem. Phys.* **1989**, *91*, 7075.
(3) Debenedetti, P. G.; Mohamed, R. S. *J. Chem. Phys.* **1989**, *90*, 4528.
(4) Eckert, C. A.; Knuston, B. L.; Debenedetti, P. G. *Nature* **1996**, *383*, 313−318.
(5) Lynden-Bell, R.; Giovambattista, N.; Debenedetti, P.; Head-Gordon, T.; Rossky, P. *Phys. Chem. Chem. Phys.* **2011**, *13*, 2366−2379.
(6) Lazaridis, T. *J. Phys. Chem. B* **1998**, *102*, 3531−3541.
(7) Lazaridis, T. *J. Phys. Chem. B* **1998**, *102*, 3542−3550.
(8) Yu, H.; Karplus, M. *J. Chem. Phys.* **1988**, *89*, 2366−2379.
(9) Schlitter, J. *Chem. Phys. Lett.* **1993**, *215*, 617−621.
(10) Schafer, H.; Mark, A. E.; van Gunsteren, W. F. *J. Chem. Phys.* **2000**, *113*, 7809−7817.
(11) Andricioaei, I.; Karplus, M. *J. Chem. Phys.* **2001**, *115*, 6289−6292.
(12) Lazaridis, T. *Acc. Chem. Res.* **2001**, *34*, 931−937.
(13) Hess, B.; van der Vegt, N. F. A. *J. Phys. Chem. B* **2006**, *110*, 17616−17626.
(14) Agarwal, M.; Kushwaha, H. R.; Chakravarty, C. *J. Phys. Chem. B* **2010**, *114*, 651−659.
(15) Nayar, D.; Agarwal, M.; Chakravarty, C. *J. Chem. Theory Comput.* **2011**, *7*, 3354−3367.
(16) Daniel, M.-C.; Astruc, D. *Chem. Rev.* **2004**, *104*, 293−346.
(17) Kiely, C. J.; Fink, J.; Brust, M.; Bethell, D.; Schiffrin, D. J. *Nature* **1998**, *396*, 444−446.
(18) Murray, C. B.; Kagan, C. R.; Bawendi, M. G. *Annu. Rev. Mater. Sci.* **2000**, *30*, 545−610.
(19) Shevchenko, E. V.; Talapin, D. V.; Kotov, N. A.; OBrien, S.; Murray, C. B. *Nature* **2006**, *439*, 55−59.
(20) Talapin, D. V.; Shevchenko, E. V.; Bodnarchuk, M. I.; Ye, X.; Chen, J.; Murray, C. B. *Nature* **2009**, *461*, 964−967.
(21) Zhang, H.; Edwards, E. W.; Wang, D.; Möhwald, H. *Phys. Chem. Chem. Phys.* **2006**, *8*, 3288−3299.
(22) Min, Y.; Akbulut, M.; Kristiansen, K.; Golan, Y.; Israelachvili, J. *Nature Mater.* **2008**, *7*, 527−538.
(23) Bishop, K. J. M.; Wilmer, C. E.; Soh, S.; Grzybowski, B. A. *Small* **2009**, *5*, 1600−1630.
(24) Qin, Y.; Fichthorn, K. A. *Phys. Rev. E* **2006**, *73*, 020401(R).
(25) Grest, G. S.; Wang, Q.; in't Veld, P.; Keffer, D. J. *J. Chem. Phys.* **2011**, *134*, 144902.
(26) Brust, M.; Walker, M.; Bethell, D.; Schiffrin, D. J.; Whyman, R. *J. Chem. Soc., Chem. Commun.* **1994**, *7*, 801−802.
(27) Sidhaye, D. S.; Prasad, B. *Chem. Phys. Lett.* **2008**, *454*, 345−349.
(28) Sidhaye, D. S.; Prasad, B. L. V. *Chem. Mater.* **2010**, *22*, 1680−1685.
(29) Ghorai, P.; Glotzer, S. *J. Phys. Chem. B* **2010**, *114*, 1918219187.
(30) Bodnarchuk, M. I.; Kovalenko, M. V.; Heiss, W.; Talapin, D. V. *J. Am. Chem. Soc.* **2010**, *132*, 1196711977.
(31) Kulkarni, G. U.; Thomas, P. J.; Rao, C. N. R. *Pure Appl. Chem.* **2002**, *74*, 1581−1591.
(32) Luedtke, W. D.; Landman, U. *J. Phys. Chem.* **1996**, *100*, 13323−13329.
(33) Luedtke, W. D.; Landman, U. *J. Phys. Chem. B* **1998**, *102*, 6566−6572.
(34) Tay, K.; Bresme, F. *Mol. Simul.* **2005**, *31*, 515−526.
(35) Schapotschnikow, P.; Vlugt, T. J. H. *J. Phys. Chem. C* **2007**, *111*, 10201−10212.
(36) Schapotschnikow, P.; Pool, R.; Vlugt, T. J. H. *Nano Lett.* **2008**, *8*, 2930−2934.
(37) Dalvi, V. H.; Srinivasan, V.; Rossky, P. J. *J. Phys. Chem. C* **2010**, *114*, 15553−15561.
(38) Dalvi, V. H.; Srinivasan, V.; Rossky, P. J. *J. Phys. Chem. C* **2010**, *114*, 15562−15573.
(39) Lal, M.; Plummer, M.; Richmond, N. J.; Smith, W. *J. Phys. Chem. B* **2004**, *108*, 6052−6061.
(40) Lal, M.; Plummer, M.; Smith, W. *J. Phys. Chem. B* **2006**, *110*, 20879−20888.
(41) Yang, Z.; Yang, X.; Xu, Z.; Yang, N. *J. Chem. Phys.* **2010**, *133*, 094702.
(42) Patel, N.; Egorov, S. A. *J. Chem. Phys.* **2007**, *126*, 054706.
(43) Fernandez, C. A.; Hoppes, E. M.; Bekhazi, J. G.; Wang, C.; Wiacek, R. J.; Warner, M. G.; Fryxell, G. E.; Bays, J. T.; Addleman, R. S. *J. Phys. Chem. C* **2008**, *112*, 13947−13957.
(44) Fernandez, C. A.; Bekhazi, J.; Hoppes, E. M.; Wiacek, R. J.; Fryxell, G. E.; Bays, J.; Warner, M. G.; Wang, C.; Hutchison, J. E.; Addleman, R. S. *Small* **2009**, *5*, 961−969.
(45) Wilson, N. T.; Johnston, R. L. *Eur. Phys. J. D* **2000**, *12*, 161−169.
(46) Sinha, S. K.; Chakraborty, S.; Bandyopadhyay, S. *Langmuir* **2011**, *26*, 9911−9916.
(47) Goel, T.; Patra, C. N.; Mukherjee, T.; Chakravarty, C. *J. Chem. Phys.* **2008**, *129*, 164904.
(48) Wallace, D. *J. Chem. Phys.* **1987**, *87*, 2282.
(49) Baranyai, A.; Evans, D. *Phys. Rev. A* **1989**, *40*, 3817−3822.
(50) Kirkwood, J.; Buff, F. *J. Chem. Phys.* **1951**, *19*, 774−777.
(51) Debenedetti, P. G. *Chem. Eng. Sci.* **1987**, *42*, 2203−2212.
(52) Martin, M. G.; Siepmann, J. I. *J. Phys. Chem. B* **1998**, *102*, 2569−2577.
(53) Leach, A. *Molecular Modelling: Principles and Applications*; Addison Wesley Longman Limited: China, 1998.
(54) Chen, B.; Siepmann, J. I. *J. Phys. Chem. B* **1999**, *103*, 5370−5379.
(55) Jorgensen, W. L.; Madura, J. D.; Swenson, C. J. *J. Am. Chem. Soc.* **1984**, *106*, 6638−6646.
(56) Ryckaert, J.-P.; Bellemans, A. *Faraday Discuss.* **1978**, *66*, 95−106.
(57) Clarke, J. H. R.; Smith, W.; Woodcock, L. V. *J. Chem. Phys.* **1986**, *84*, 2290−2294.
(58) Sellers, H.; Ulman, A.; Shnidman, Y.; Eilers, J. E. *J. Am. Chem. Soc.* **1993**, *115*, 9389−9401.
(59) *Birmingham Cluster Web*, http://www.tc.bham.ac.uk/bcweb (accessed May 25, 2012). The structure of Au38 was downloaded from this website.
(60) Martinez, J. M.; Martinez, L. *J. Comput. Chem.* **2003**, *24*, 819−825.
(61) Smith, W.; Yong, C. W.; Rodger, P. M. *Mol. Simulat.* **2002**, *28*, 385−471. The DLPOLY website is http://www.cse.clrc.ac.uk/msi/software/DL_POLY (accessed May 1, 2012).
(62) Tuckerman, M. E.; Martyna, G. J.; Berne, B. J. *J. Chem. Phys.* **1990**, *93*, 1287−1291.
(63) Batista, R. J. C.; Mazzoni, M. S. C.; Chacham, S. *Nanotechnology* **2010**, *21*, 065705.